The EMBO Journal vol.15 no.16 pp.4246–4253, 1996

Imaging the intracellular trafficking and state of the AB_5 quaternary structure of cholera toxin

Philippe I.H.Bastiaens, Irina V.Majoul[1], Peter J.Verveer, Hans-Dieter Söling[1] and Thomas M.Jovin[2]

Department of Molecular Biology, Max Planck Institute for Biophysical Chemistry, Postfach 2841, D-37018 Göttingen and [1]Department of Clinical Biochemistry, Göttingen University, Robert-Koch Strasse 40, D-37070 Göttingen, Germany

[2]Corresponding author

The subcellular localization and corresponding quaternary state of fluorescent labelled cholera toxin were determined at different time points after exposure to living cells by a novel form of fluorescence confocal microscopy. The compartmentalization and locus of separation of the pentameric B subunits (CTB) from the A subunit (CTA) of the toxin were evaluated on a pixel-by-pixel (voxel-by-voxel) basis by measuring the fluorescence resonance energy transfer (FRET) between CTB labelled with the sulfoindocyanine dye Cy3 and an antibody against CTA labelled with Cy5. The FRET efficiency was determined by a new technique based on the release of quenching of the Cy3 donor after photodestruction of the Cy5 acceptor in a region of interest within the cell. The results demonstrate vesicular transport of the holotoxin from the plasma membrane to the Golgi compartment with subsequent separation of the CTA and CTB subunits. The CTA subunit is redirected to the plasma membrane by retrograde transport via the endoplasmic reticulum whereas the CTB subunit persists in the Golgi compartment.

Keywords: ADP-ribosylation/confocal microscopy/ fluorescence resonance energy transfer/photobleaching

Introduction

The disease cholera is a major affliction of the human race, reaching epidemic proportions in large populations of the world. The acute dehydration (Gill, 1977; Field *et al.*, 1989) that occurs after colonization of the intestinal mucosa with *Vibrio cholerae* is induced by cholera toxin (CTX) (Spangler, 1992), which has an AB_5 oligomeric structure consisting of one 28.5 kDa CTA subunit (a disulfide dimer of A1 and A2 peptides) embedded in an isopentamer of 11 kDa CTB subunits (Gill, 1976; Mekalanos *et al.*, 1979). The holotoxin binds to the cell surface via interactions of CTB with ganglioside G_{M1} (van Heyningen, 1974). After internalization and processing, CTB and CTA dissociate, followed by reductive cleavage of CTA with liberation of the enzymatically active A1 peptide. The latter ADP-ribosylates the α subunits of heterotrimeric G_S proteins (Cassel and Selinger, 1977; Cassel and Pfeuffer, 1978; Galloway and Heyningen, 1987), leading to a persistent activation of adenylate cyclase.

The process by which CTX enters the cell and is translocated to its site of action remains obscure, although vesicular traffic (Lencer *et al.*, 1995) and a functional Golgi compartment (Nambiar *et al.*, 1993; Orlandi *et al.*, 1993; Lencer *et al.*, 1995) have been implicated. Internalization is presumably into non-coated vesicles (Tran *et al.*, 1987), generated via caveoli (Parton, 1994; Parton *et al.*, 1994) or the endosomal pathway (Sofer and Futerman, 1995). A major question relates to the locus and mechanism of toxin disassembly into its constituent subunits. We have applied a novel form of fluorescence laser scanning confocal microscopy (Bastiaens *et al.*, 1996) that yields a three-dimensional evaluation of protein–protein interactions in cells, in order to study the intracellular localization and corresponding quaternary state of CTX after initial binding to the plasma membrane. A fluorescent donor–acceptor pair was attached to CTB and CTA in order to generate a fluorescence resonance energy transfer (FRET) signal in the holotoxin, the abolition of which denotes a dissociation into the constituent subunits. The FRET efficiency characteristically varies with the sixth power of the donor–acceptor separation (Förster, 1948) over a range of 1–10 nm corresponding to typical macromolecular dimensions (Figure 1). The quaternary state of the toxin can thus be followed on and within a cell by measuring FRET pixel-by-pixel (two-dimensionally) or voxel-by-voxel (three-dimensionally) in the microscope (Jovin and Arndt-Jovin, 1989; Gadella *et al.*, 1993, 1994; Tsien *et al.*, 1993; Bastiaens *et al.*, 1996; Clegg, 1995; Gadella and Jovin, 1995).

Results

FRET by acceptor and donor photobleaching

We have recently devised a new method for evaluating FRET in the laser scanning confocal microscope based on the increase of the donor quantum yield (reflected in the measured emission intensity) after photochemical destruction of the energy acceptor in a specific portion of the cell with the aim of annulling its quenching effect on the donor (Bastiaens *et al.*, 1996). The FRET efficiency within the selected region of interest is computed from the ratio of the two donor fluorescence images before and after bleaching (Figure 1). An additional independent determination of the FRET efficiency can be made from the measurement of donor photobleaching kinetics according to the method of photobleaching digital imaging microscopy (pbDIM) (Jovin and Arndt-Jovin, 1989; Bastiaens *et al.*, 1996; Gadella and Jovin, 1995). In pbDIM one exploits the phenomenon that the photobleaching time (τ_{bl}) is inversely proportional to the fluorescence lifetime of a compound. This implies that a process leading to a

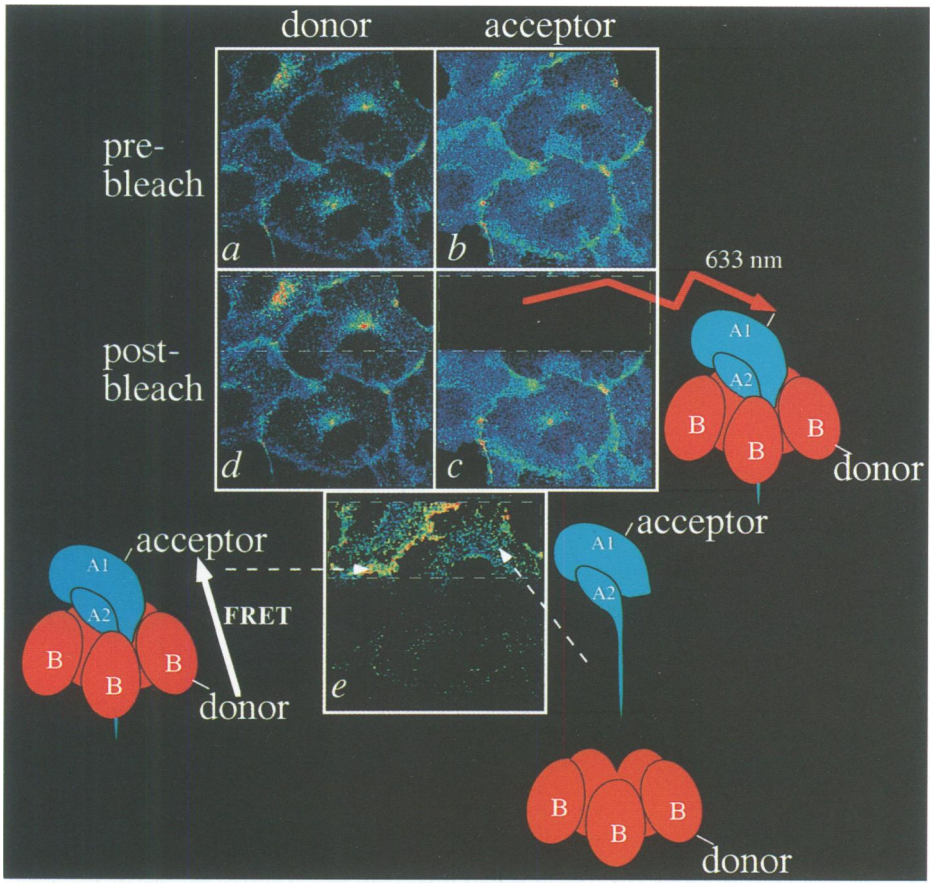

Fig. 1. Principle of acceptor photobleaching FRET microscopy to detect cholera subunit separation *in situ*. (**a**) Donor fluorescence image and (**b**) acceptor fluorescence image are taken, after which (**c**), the acceptor probe is photodestroyed by irradiation with 633 nm light in a selected portion of the cell. (**d**) A donor fluorescence image is obtained after acceptor photodestruction. (**e**) Pixel-by-pixel FRET efficiencies are calculated from the image arithmetic operation (d–a)/d. Any drift in image position is found by calculating the location of the maximum in the cross-correlation between image (a) and (d). Image (d) is then translated to correct for the drift (typically 1–2 pixels along the *x* and *y* axes) before the FRET calculation. FRET from donor on the CTB subunit to the acceptor on the CTA subunit is substantial in regions of the cell containing holotoxin. Subunit separation causes the average distance between donor on the CTB subunit and acceptor on the CTA subunit to exceed the limit (~7.2 nm) for detectable FRET (>10% efficiency). The example features a group of cells 30 min after initiation of uptake of fluorescent labelled toxin.

shortened lifetime of the excited state (such as FRET) will cause the τ_{bl} of the fluorophore to increase proportionally. Photobleaching times can be determined on a pixel-by-pixel basis with relative ease in the microscope, thereby mapping the energy transfer efficiency throughout the cell. However, the calculation of the FRET efficiency requires the measurement of a reference donor photobleaching time obtained in the absence of the acceptor. One can circumvent the recourse to a separate sample by bringing about the specific photodestruction of the acceptor molecule in a region of interest, as described in the acceptor photodestruction method above. By then performing the measurement of donor photobleaching kinetics, a determination of the FRET efficiency can be made using the acceptor-depleted region to provide the required reference photobleaching time (see Figure 4).

Fluorescence labelling of cholera holotoxin and anti-CTA antibody

To apply these techniques to the study of the compartmentalization and locus-specific processing of CTX in cells, we labelled the protein covalently with the succinimide ester of the fluorescent sulfoindocyanine dye Cy3 (Southwick *et al.*, 1990). Resolution of the denatured toxin on SDS–PAGE revealed that CTB, but not CTA, was labelled (Majoul *et al.*, 1996), with an average of one Cy3 molecule per CTB-subunit (Cy3–CTB). An energy acceptor probe specific for CTA was devised by labelling the IgG fraction of rabbit anti-CTA antiserum with the succinimide ester of the sulfoindocyanine dye Cy5 (Cy5–α-CTA) (Southwick *et al.*, 1990); the mean labelling stoichiometry was three Cy5 moieties per IgG. The antibody preparation was monospecific for CTA on Western blots and recognized CTA in toxin-treated Vero cells, a monkey kidney tumour cell line (Figure 2, second column). No fluorescence was detected in control cells not exposed to CTX.

Intracellular redistribution and processing of cholera holotoxin

Vero cells were treated with labelled CTX and the distribution of the CTB subunits (pentameric oligomer or individual molecules; signal from Cy3–CTB) and of the CTA subunit (signal from Cy5–α-CTA) were followed in time by confocal fluorescence microscopy. The quaternary state of the labelled CTX in the cells was assessed by measuring FRET in a region of interest (Figure 2). The normalized Cy5/Cy3 (A/B) ratio images were also determined

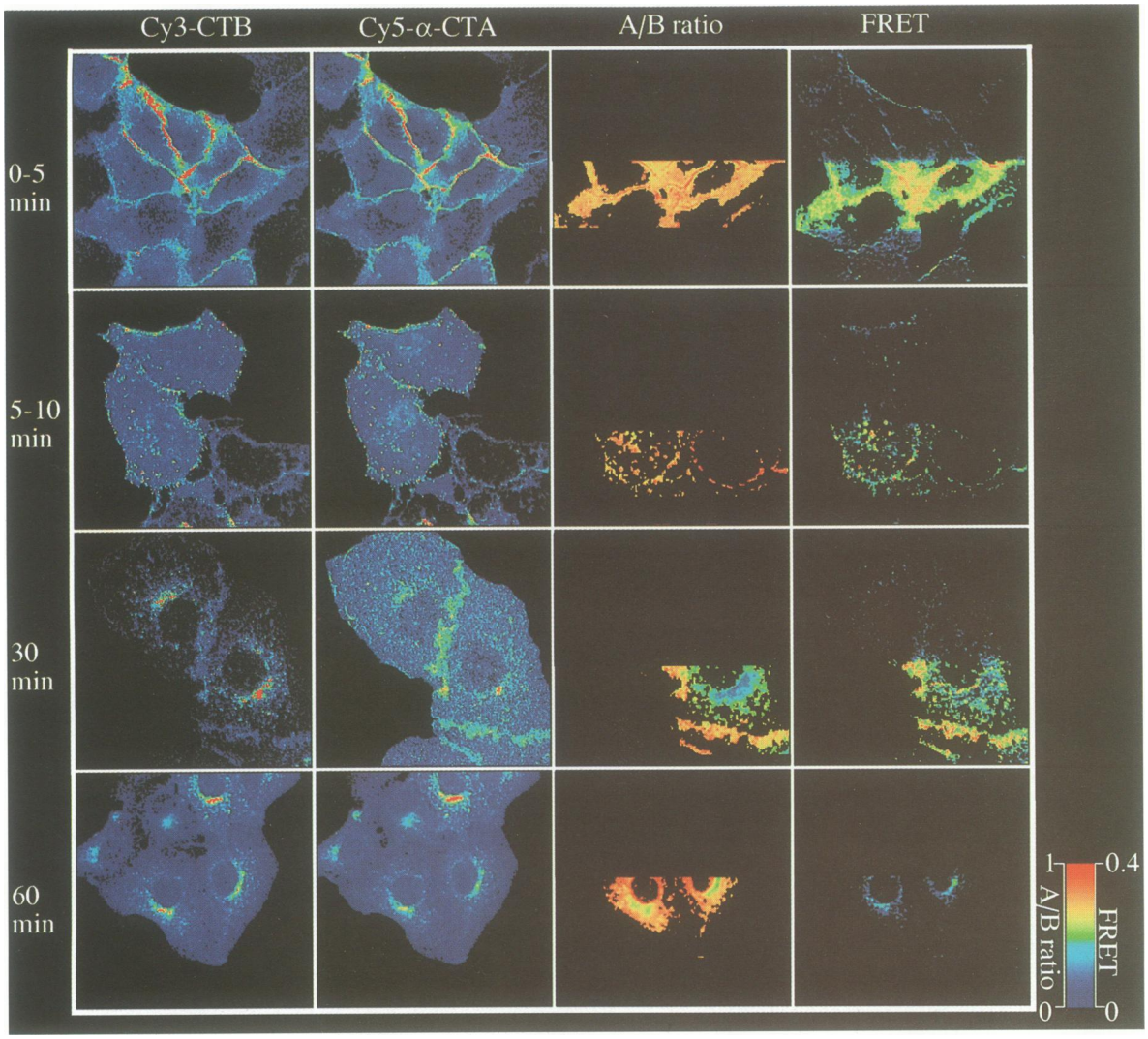

Fig. 2. Time-dependent cellular localization and molecular proximity of CTA and CTB subunits of cholera toxin. The incubation times at 37°C are indicated. Column 1: Cy3–CTB fluorescence. Column 2: Cy5–α-CTA fluorescence. Column 3: normalized fluorescence ratio Cy5/Cy3 (image arithmetic b/d, see Figure 1) restricted to regions of Cy5 photodestruction. Column 4: FRET efficiency.

(Figure 2, A/B ratio) and the correlation with the corresponding FRET efficiencies established at every time point in the form of two-dimensional histograms (Figure 3a–d). The time-dependent redistribution and processing of the toxin were as follows.

0–5 min. Upon binding to the external surface of the plasma membrane, the fluorescence signals exhibited a tight distribution both in A/B ratio and FRET efficiency (Figure 2, top row and Figure 3a) which we interpret as co-localized equimolar CTA and CTB pentamers in the holotoxin quaternary structure. The FRET values represent a calibration for the molecular proximity (nm scale) signals. Thus, the FRET efficiency (0.28 ± 0.06) observed in Figure 3a corresponds to the intact AB_5 quaternary structure, and we assume that at subsequent time points the calculated FRET efficiencies are proportional to the molar fraction of Cy3–CTB in the form of holotoxin. That is, if the CTB pentamer dissociates from CTA in a single step process, the fraction of holotoxin at every pixel is given by the FRET efficiency divided by 0.28.

5–10 min. An uptake of toxin into vesicular structures ensued, most of which maintained a uniform A/B ratio and FRET efficiency (0.28) corresponding to holotoxin (Figure 2, second row; Figure 3b). In a minor population of vesicles containing 27% of the toxin according to integrated fluorescence intensity, lower FRET efficiencies (<0.2) were also observed, the A/B ratio remaining constant. We infer that in this vesicle subpopulation, some degree of subunit dissociation had taken place.

30 min. A more dramatic heterogeneity in the internalized toxin population was apparent at the time corresponding to the onset of the cAMP increase in the cells (Nambiar *et al.*, 1993; Orlandi *et al.*, 1993; Majoul *et al.*, 1996). There was a predominant localization of the Cy3 signal in the Golgi apparatus (Figure 2, third row), identified by a monoclonal antibody against giantin (Majoul *et al.*, 1996). In contrast, the Cy5 signal originated not only from the Golgi but also to a lesser extent from the endoplasmic reticulum (ER), identified by a polyclonal antibody against calreticulin (Majoul *et al.*, 1996), as well as the plasma membrane. Lower values for the A/B ratio in the Golgi indicated a preferential retention of CTB and/or relocaliz-

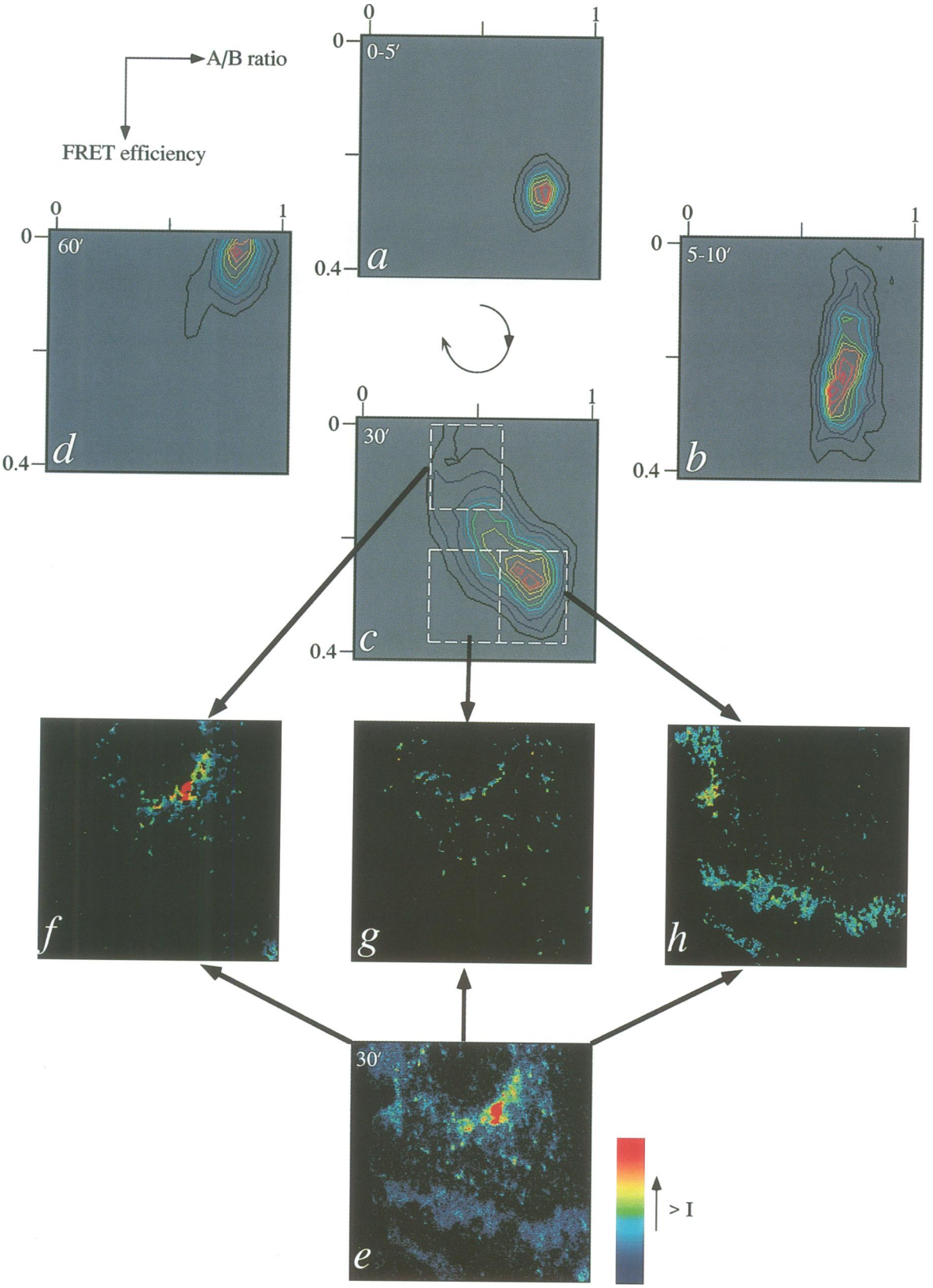

Fig. 3. Spatial correlation between FRET efficiency and Cy5/Cy3 fluorescence ratio. (**a–d**) Two-dimensional histograms of FRET and A/B ratios of the cells at different time points after toxin internalization shown in Figure 2. The normalized A/B ranges for the time points were linear but not scaled equally in the experiments shown here. The three regions in histogram (c) (bounded by white rectangles) were used to calculate masks in the original Cy3 fluorescence image (**e**; B subunits) in order to disentangle cellular regions with toxin in different molecular states. Regions in the cell with: (**f**) low FRET and low A/B ratios; (**g**) high FRET and low A/B ratios; (**h**) high FRET and high A/B ratios.

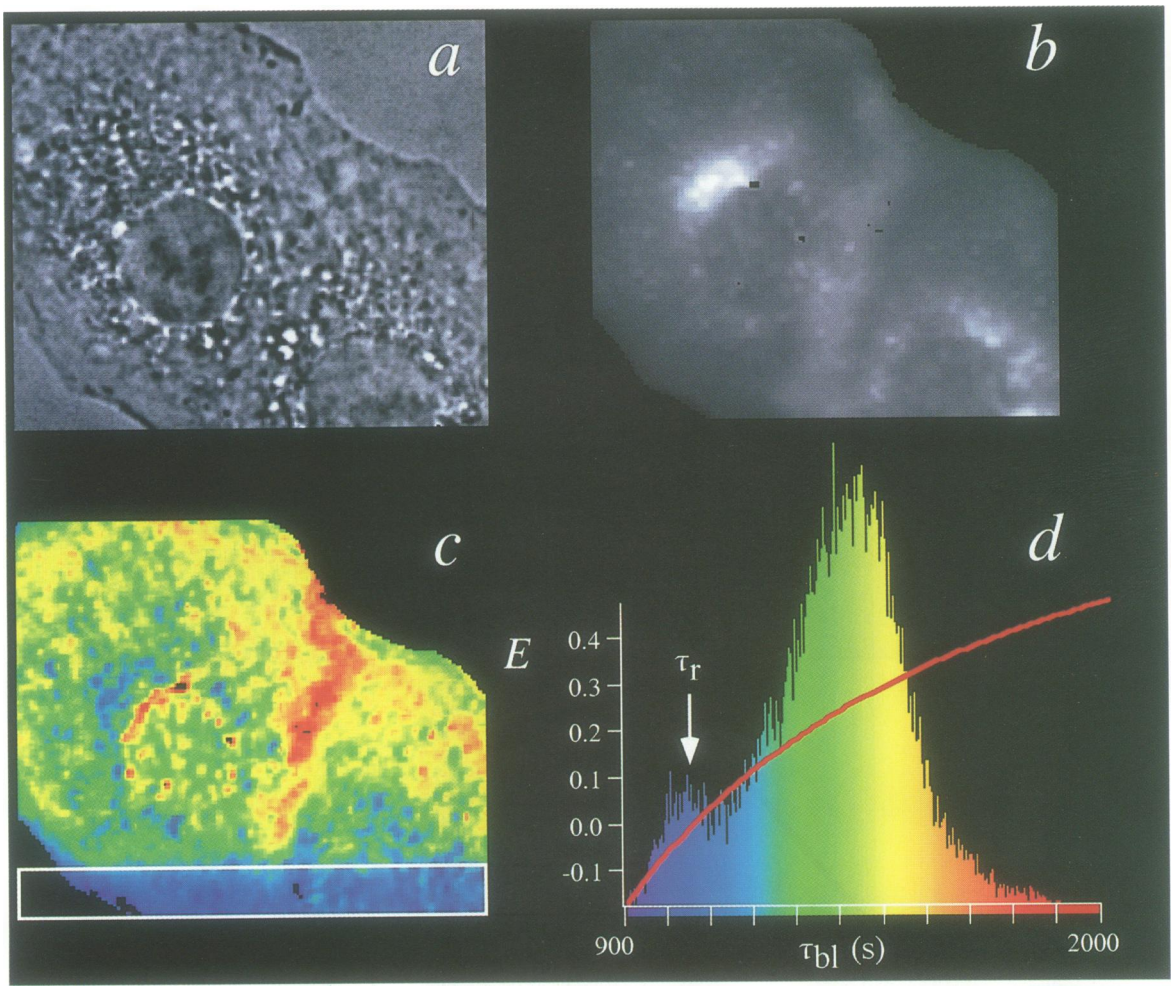

Fig. 4. FRET by donor photobleaching with or without acceptor photodestruction. The example features cells of Figure 2 seen 30 min after the start of CTX uptake. (**a**) Phase contrast images. (**b**) Fluorescence amplitude of Cy3–CTB. (**c**) Pseudocolour map of donor photobleaching times ($\tau_{bl,\,i}$). The reference region in which Cy5 was photodestroyed by 633 nm illumination is enclosed by a rectangle bounded by white. (**d**) Histogram and pseudocolour representation of donor photobleaching times and calculated FRET efficiencies (*E*, red curve). The white arrow indicates the mean reference photobleaching time constant (τ_r). *E* was calculated from the corresponding photobleaching time constants (τ_{bl}) of Cy3 (donor) in the presence of Cy5 (acceptor) according to the expression $E = 1-\tau_r/\tau_{bl}$.

ation of CTA in the other compartments. According to the FRET efficiency map (Figure 2, third row), some holotoxin remained on the plasma membrane, presumably corresponding to attached but non-internalized toxin. In addition, holotoxin was present in vesicles and the perinuclear Golgi region (see also below). The low FRET efficiencies in the rest of the Golgi indicated that dissociation of the CTA and CTB subunits had occurred.

Three domains of the two-dimensional histogram (Figure 3c) were selected and used as masks for identifying the corresponding regions (Figure 3f–h) in the original donor (Cy3–CTB) intensity distribution image (Figure 3e). The domain in the histogram corresponding to high ratios and high FRET efficiencies clearly mapped to the membrane regions of the cells (Figure 3h). The ~0.3 FRET efficiency indicated that the signals originated from non-internalized holotoxin, whereas the high A/B ratio arose from the co-localization with dissociated CTA subunit that had been intracellularly processed and translocated to the membrane. Because of the high FRET efficiencies, we ascribe the region in the histogram with lower A/B ratios to the AB_5 holotoxin; it mapped to vesicular structures and the perinuclear Golgi region (Figure 3g). The latter image depicts the transport of holotoxin in vesicular structures from the plasma membrane to the perinuclear Golgi. The low FRET efficiencies and lower A/B ratios mapped to the Golgi and some vesicular structures (Figure 3f). The CTA and CTB subunits were separated in these compartments.

60 min. Rather uniform A/B ratios and low FRET efficiencies were observed throughout the cell at this late time point (Figure 2, bottom row and Figure 3d). A small fraction of unprocessed holotoxin remained in the Golgi, as evidenced by finite FRET efficiencies (Figures 2 and 3d).

An independent donor photobleaching experiment was performed on the cells shown in Figure 2, 30 min after toxin administration. In this case, the region in which the acceptor was photodestroyed constituted the reference region for the calculation of FRET efficiency (Figure 4). A distribution of FRET efficiency was evident in the complementary (top) region of the cells, as shown from photobleaching times longer than those in the acceptor-depleted (reference) region (Figure 4c and d). From the

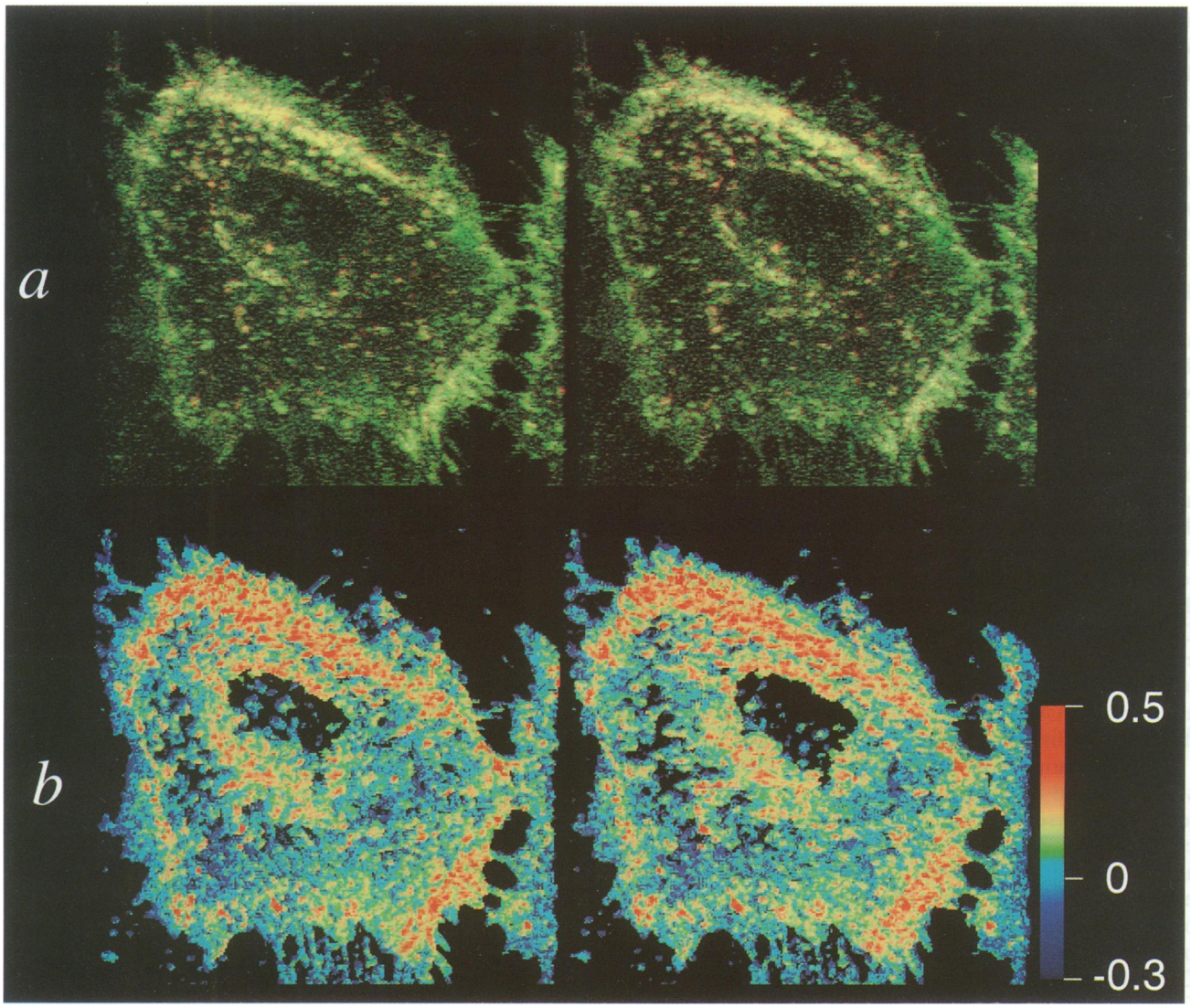

Fig. 5. Stereo images of three-dimensional reconstructed distributions of CTA, CTB, and FRET efficiencies. Vero cells, 30 min of uptake of labelled CTX. (**a**) Red–green colour coding of Cy3–CTB (red) and Cy5–α-CTA (green). (**b**) False colour coding of FRET efficiency; the negative values reflect the statistical spread about zero. The black regions are thresholded areas lacking significant Cy3 fluorescence. The FRET efficiency was calculated by the three-dimensional equivalence of the image arithmetic operation given in the legend of Figure 1. See Materials and methods for procedures.

photobleaching times and calculated FRET efficiencies in the cell we conclude that holotoxin was again apparent in the plasma membrane, vesicular structures and perinuclear Golgi region (yellow–red structures), with separated toxin subunits elsewhere in the Golgi and in other vesicles (blue structures). These experiments demonstrated that the independent FRET determinations by the acceptor photodestruction and by donor photobleaching kinetics compared very well.

Three-dimensional distribution of intracellular cholera toxin

In order to obtain a more defined picture of the CTX distribution and quaternary state within cellular compartments, cells at the critical time of 30 min after initiation of toxin uptake (onset of cAMP formation) were scanned at high resolution in three dimensions. The three-dimensional data sets obtained with the confocal microscope were restored with a new algorithm which significantly enhances resolution (see Materials and methods). The FRET efficiencies were determined by the acceptor photodestruction method described in Figure 1. The distributions of CTA and CTB and of the corresponding calculated FRET efficiencies are shown as stereo images in Figure 5. CTA and CTB co-localized in the perinuclear, vesicular and plasma membrane structures (Figure 5a, yellow structures) and exhibited high FRET efficiencies (0.3–0.4, Figure 5b). The reddish colour in vesicles about the nucleus (Figure 5a) indicates the accumulation of CTB whereas the green colour associated with the basal plasma membrane reflects the translocation of CTA. The ruffled appearance of the plasma membrane was due to the retraction of the cells in response to toxin-induced loss of water.

Discussion

Confocal laser scanning microscopy with Cy3–CTB and Cy5–α-CTA enabled the time-dependent localization of

the toxin subunits within the subcellular compartments of Vero cells. In addition, the measurement of FRET between the Cy3 (donor) and Cy5 (acceptor) labels permitted the evaluation of the quaternary state of the toxin at every pixel (voxel). Two independent photobleaching methods for the determination of FRET efficiencies within the cell were used: donor photobleaching kinetics; and release of quenching by acceptor photodestruction. The latter technique, introduced here as a simple procedure in the confocal microscope, was validated by virtue of the quantitative agreement between the two methods.

One might wish to question the use of a labelled antibody for the detection of CTA since dissociation of the complex or hindered binding to the AB_5 holotoxin would lead to an incorrect interpretation of data, i.e. that CTA was being dissociated from CTB. However, the large measured FRET signals were unambiguous indicators of molecular proximity, constituting strong evidence that holotoxin was present in internalized vesicles and in the perinuclear part of the Golgi apparatus. Both high (perinuclear area, holotoxin) and low (more outward regions) FRET efficiencies were observed reproducibly in the Golgi in combination with relatively constant Cy5/Cy3 signal ratios. This finding indicates that the CTA epitope was recognized by the antibody with or without it being in molecular proximity to the CTB subunit, thus arguing against the loss of epitope recognition under different conditions.

We summarize the results of this and the companion study (Majoul *et al.*, 1996) by outlining the following temporal course of cholera toxin interactions with Vero cells: (i) The holotoxin binds to the plasma membrane and is internalized into vesicles with preservation of the native AB_5 oligomeric structure. (ii) The vesicular traffic of CTX is directed to a Golgi compartment, where most of the toxin arrives in the AB_5 form. (iii) The CTA and CTB subunits separate in the perinuclear region of the Golgi cisternea. (iv) CTA undergoes retrograde transport from the Golgi to the ER through an intermediate compartment, while CTB persists in the Golgi and is later degraded in lysosomes. Finally, in step (v) intact CTA or the A1 polypeptide is translocated from the ER to the cytosol by an as yet unknown mechanism. Finally, the A1 polypeptide ADP-ribosylates $G_{S\alpha}$ subunits at the plasma membrane. During the review process of this report one of the referees suggested an alternative mechanism involving a rapid translocation of the holotoxin from the Golgi to the ER followed by rapid dissociation and anterograde transport of CTB back to the Golgi. Inasmuch as we did not detect significant amounts of CTB subunit in the ER, either biochemically (Majoul *et al.*, 1996) or cytochemically (this study), the proposed mechanism appears implausible on kinetic grounds. Furthermore, direct evidence for a retrograde microtubule-dependent transport of CTA from the Golgi to the ER was obtained (Majoul *et al.*, 1996).

In conclusion, the study by photobleaching microscopy of cells exposed to fluorescent labelled CTX is prototypic for investigations of protein redistribution and protein–protein interactions *in situ*. New information about the intracellular compartmentalization and corresponding quaternary states of the toxin were obtained without recourse to cellular fractionation techniques. The methodology presented here has been shown to be effective in studies of living cells and of signal transduction mechanisms (Bastiaens and Jovin, 1996) and metabolic pathways (Bastiaens *et al.*, 1996) in particular. The novel FRET determination based on acceptor photodestruction is particularly suited to the confocal fluorescence microscope and does not require external calibration. Data analysis of the FRET and signal ratio images in combination with two-dimensional histograms (Demandolx and Davoust, 1996) provides a unique tool for the differentiation of cellular compartments with respect to the stoichiometry and molecular states of oligomeric and multidomain proteins.

Materials and methods

Protein labelling with Cy3 and Cy5

α-CTA and CTX were reacted in 0.1 M bicine–NaOH (α-CTA, pH 9.0; CTX, pH 8.0) for 30 min at room temperature with a 10-fold molar excess of Cy5.29-OSu and Cy3.29-OSu (Biological Detection Systems), respectively. Excess dye was removed by gel filtration and labelled protein concentrated to 0.5–1 mg/ml in a Centricon 30 (Amicon) in PBS.

Cellular incubation with labelled cholera holotoxin

Vero cells were pretreated at 0°C for 20 min with 1 M G_{M1} in DMEM without FCS before incubation with 0.1 μg/ml labelled toxin (0°C, 20 min). The cells were transferred to DMEM containing 10% FCS at 37°C, 5% CO_2 to start toxin internalization after unbound CTX had been removed by washing in the presence of 1 μM G_{M1}. At the time points given, cells were fixed in 0.2% glutaraldehyde/2% paraformaldehyde (10 min, 0°C; 30 min, room temperature), quenched in 50 mM NH_4Cl followed by permeabilization in 0.15% saponin in PBS/0.2% gelatin. The cells were incubated for 30 min at 37°C with Cy5–α-CTA, washed and mounted in 0.1 M Tris–HCl, 25% (w/v) glycerol and 10% (w/v) Mowiol 4-88 (Hoechst).

Confocal laser scanning microscopy and acceptor photobleaching

Confocal microscopy was with a Zeiss LSM10 system, 40×, 1.3 NA oil immersion objective. Cy3: excitation at 514 nm, emission selected through Omega 590BP35 filter. Cy5: excitation at 633 nm, emission selected through an LP665 filter. Images were acquired with the CLSM. For acceptor photobleaching, the 633 nm laser was coupled to an accousto-optical modulator (AOM) so as to define a region of interest within which the scanning at full power led to total photobleaching of the Cy5 acceptor.

FRET microscopy by donor photobleaching

Irradiation on a Zeiss Axioplan microscope (objective: 40×, 1.3 NA oil immersion) was at 546 nm with an Osram HBO 100 W Hg lamp (filters: Zeiss 546BP12 bandpass and Omega FT580 dichroic). Cy3 fluorescence images were collected through a Corion SS600 bandpass filter with a slow-scan Photometrics Series 200 CCD camera (Kodak KAF 1400, 12-bit ADC) interfaced to a Macintosh Quadra 800 computer. The specimens were bleached by constant illumination and 61 micrographs were acquired by opening the camera shutter on the camera at fixed time intervals. Acquisition times were optimized for the full dynamic range of the CCD camera. The pixel-by-pixel photobleaching decay data were exported and fitted to a single exponential + offset model by the program DECAY (Gadella and Jovin, 1995), thereby generating images of the photobleaching time constants ($\tau_{bl,i}$), amplitudes, and residual backgrounds for significant pixels i. The $\tau_{bl,i}$ images were 8-bit encoded and processed with NIH-Image (National Institutes of Health, Bethesda, MA) to generate pseudocolour representations.

Three-dimensional image reconstruction

Confocal microscopy was performed as given in the legend of Figure 2 except that a 63×, 1.4 NA oil immersion objective was used. Twenty optical sections (0.2 μm apart) of donor and acceptor fluorescence were recorded, after which the acceptor was photodestroyed in the displayed cell by irradiation at 633 nm and a second stack of 20 sections of donor fluorescence recorded. Registration of the three-dimensional donor image stacks before and after bleaching was accomplished by calculating the location of the maximum in the three-dimensional cross-correlation

function and translating the post-bleaching donor stack accordingly. Image deconvolution was performed by an algorithm (P.J.Verveer and T.M.Jovin, manuscript in preparation) based on the constrained minimization of the same regularized χ^2 criterion given by Carrington *et al.* (1995). This algorithm uses (i) the prior knowledge that fluorescence intensities are non-negative, and (ii) a calculated point spread function. After reconstruction, the images were scaled by normalizing the integrated image intensities to the original values. The FRET efficiencies were calculated after smoothing in the x and y directions using a 3×3 uniform filter.

References

Bastiaens,P.I.H. and Jovin,T.M. (1996) Microspectroscopic imaging tracks the intracellular processing of a signal transduction protein: fluorescent labeled protein kinase C βI. *Proc. Natl Acad. Sci. USA*, in press.

Bastiaens,P.I.H., Wouters,F.S. and Jovin,T.M. (1996) Imaging the molecular state of proteins in cells by fluorescence resonance energy transfer (FRET). Sequential photobleaching of Förster donor-acceptor pairs. *Proceedings of the Second Hamamatsu International Symposium on Biomolecular Mechanisms and Photonics: Cell–Cell Communication*. Hamamatsu Photonics, K.K., in press.

Carrington,W.A., Lynch,R.M., Moore,E.D.W., Isenberg,G., Fogarty,K.E. and Fay,F.S. (1995) Superresolution three-dimensional images of fluorescence in cells with minimal light exposure. *Science*, **268**, 1483–1487.

Cassel,D. and Pfeuffer,T. (1978) Mechanism of cholera toxin action: covalent modification of the guanyl nucleotide-binding protein of the adenylate cyclase system. *Proc. Natl Acad. Sci. USA*, **75**, 2669–2673.

Cassel,D. and Selinger,Z. (1977) Mechanism of adenylate cyclase activation by cholera toxin: inhibition of GTP hydrolysis at the regulatory site. *Proc. Natl Acad. Sci. USA*, **74**, 3307–3311.

Clegg,R.M. (1995) Fluorescence resonance energy transfer. *Curr. Opin. Biotechnol.*, **6**, 103–110.

Demandolx,D. and Davoust,J. (1996) Subcellular cytofluorometry in confocal microscopy. In Slavik,J. (ed.), *Fluorescence Microscopy and Fluorescence Probes*. Plenum Press, New York, in press.

Field,M., Rao,M.C. and Chang,E.B. (1989) Intestinal electrolyte transport and diarrheal disease I. *N. Engl. J. Med.*, **321**, 800–806.

Förster,T. (1948) Zwischenmolekulare Energiewanderung und Fluoreszenz. *Ann. Physik.*, **2**, 55–75.

Gadella,T.W.J.,Jr and Jovin,T.M. (1995) Oligomerization of epidermal growth factor receptors (EGFR) on A431 cells studied by time-resolved fluorescence imaging microscopy. A stereochemical model for tyrosine kinase receptor activation. *J. Cell Biol.*, **129**, 1543–1558.

Gadella,T.W.J.,Jr, Jovin,T.M. and Clegg,R.M. (1993) Fluorescence lifetime imaging microscopy (FLIM): spatial resolution of microstructures on the nanosecond time scale. *Biophys. Chem.*, **48**, 221–239.

Gadella,T.W.J.,Jr, Clegg,R.M. and Jovin,T.M. (1994) Fluorescence lifetime imaging microscopy: pixel-by-pixel analysis of phase-modulation data. *Bioimaging*, **2**, 139–159.

Galloway,T.S. and Heyningen,S. (1987) Binding of NAD^+ by cholera toxin. *Biochem. J.*, **244**, 225–230.

Gill,D.M. (1976) The arrangement of subunits of cholera toxin. *Biochemistry*, **15**, 1242–1248.

Gill,D.M. (1977) Mechanism of action of cholera toxin. *Adv. Cyclic Nucleotide Res.*, **8**, 85–118.

Jovin,T.M. and Arndt-Jovin,D.J. (1989) FRET microscopy: digital imaging of fluorescence resonance energy transfer. Application in cell biology. In Kohen,E., Ploem,J.S. and Hirschberg,J.G. (eds), *Cell Structure and Function by Microspectrofluorimetry*. Academic Press, Orlando, FL, pp. 99–117.

Lencer,W.I., Moe,S., Rufo,P.A. and Madara,J.L. (1995) Transcytosis of cholera toxin subunits across model human intestinal epithelia. *Proc. Natl Acad. Sci. USA*, **92**, 10094–10098.

Majoul,I.V., Bastiaens,P.I.H. and Söling,H.D. (1996) Transport of an external KDEL-protein from the plasma membrane to the endoplasmic reticulum. Studies with cholera toxin in Vero cells. *J. Cell Biol.*, **133**, 777–789.

Mekalanos,J.J., Collier,R.J. and Romig,W.R. (1979) Enzymic activity of cholera toxin. II Relationship to proteolytic processing, disulfide bond reduction and subunit composition. *J. Biol. Chem.*, **254**, 5855–5861.

Nambiar,M.P., Oda,T., Chen,C., Kuwazuru,Y. and Wu,H.C. (1993) Involvement of the Golgi region in the intracellular trafficking of cholera toxin. *J. Cell Physiol.*, **154**, 222–228.

Orlandi,P.A., Curran,P.K. and Fishman,P.H. (1993) Brefeldin A blocks the response of cultured cells to cholera toxin. Implications for intracellular trafficking in toxin action. *J. Biol. Chem.*, **268**, 12010–12016.

Parton,R.G. (1994) Ultrastructural localization of gangliosides: GM1 is concentrated in caveoli. *J. Histochem. Cytochem.*, **42**, 155–166.

Parton,R.G., Joggerst,B. and Simons,K. (1994) Regulated internalization of caveolae. *J. Cell Biol.*, **127**, 1199–1215.

Sofer,A. and Futerman,A.H. (1995) Cationic amphiphilic drugs inhibit the internalization of cholera toxin to the Golgi apparatus and the subsequent elevation of cyclic AMP. *J. Biol. Chem.*, **270**, 12117–12122.

Southwick,P.L., Ernst,L.A., Tauriello,E.W., Parker,S.R., Mujumdar,R.B., Mujumdar,S.R., Clever,H.A. and Waggoner,A.S. (1990) Cyanine dye labeling reagents-carboxymethylindocyanine succinimidyl esters. *Cytometry*, **11**, 418–430.

Spangler,B.D. (1992) Structure and function of cholera toxin and the related *Escherichia coli* heat-labile enterotoxin. *Microbiol. Rev.*, **56**, 622–647.

Tran,D., Carpentier,J.L., Sawano,F., Gordon,P. and Orci,L. (1987) Ligand internalized through coated or noncoated invaginations follow a common intracellular pathway. *Proc. Natl Acad. Sci. USA*, **84**, 7957–7961.

Tsien,R.Y., Bacskai,B.J. and Adams,S.R. (1993) FRET for studying intracellular signalling. *Trends Cell Biol.*, **3**, 242–245.

van Heyningen,S. (1974) Cholera toxin: interaction of subunits with ganglioside GM_1. *Science*, **183**, 656–657.

Received on December 18, 1995; revised on March 6, 1996